The Influence of Leads in Sea Ice on the Temperature of the Atmospheric Boundary Layer During Polar Night

C. Lüpkes,[1] T. Vihma,[2] G. Birnbaum,[1] U. Wacker[1]

C. Lüpkes, Alfred Wegener Institute for Polar and Marine Research, Postfach 120161, D-27515 Bremerhaven, Germany. (Christof.Luepkes@awi.de)

[1]Alfred Wegener Institute for Polar and Marine Research, Bremerhaven, Germany

[2]Finnish Meteorological Institute, Helsinki, Finland

The maximum effect of open leads within sea ice on the near-surface atmospheric temperature is estimated using a 1D atmospheric model coupled with a thermodynamic snow/sea ice model. The study is restricted to clear-sky conditions during polar night. The model is initialized with a typical wintertime atmospheric temperature profile. Results are analyzed at different integration times corresponding to different fetches over the fractured sea ice as a function of wind speed and sea ice concentration A. The results demonstrate that for $A > 90$ % small changes in the sea ice fraction have a strong effect on the near-surface temperature. A change by 1 % causes a temperature signal of up to 3.5 K. A threshold value of about 4 m s^{-1} for the 10-m wind speed divides the air-ice interaction process into a weak-wind and strong-wind regime.

1. Introduction

It is essential for climate and weather prediction models that the processes contributing to the surface energy budget are well represented. Many modeling and observational studies have been carried out in the past to investigate these processes in polar regions above sea ice [e.g., *Maykut and Untersteiner*, 1971; *Ebert and Curry*, 1993; *Sorteberg et al.* 2007] and it has been shown that one of the most important influencing factors is the sea ice concentration. However, there is still a large uncertainty on both the observed and modeled sea ice concentration [*ACIA-report*, 2005]. *Sorteberg et al.* [2007] studied the Arctic surface energy budget as simulated with 20 different models for the IPCC (Intergovernmental Panel on Climate Change). They showed that the scatter of modeled radiative and turbulent fluxes is large (scatter in the turbulent fluxes larger than the absolute values) with the most significant differences in the marginal sea ice zones, where the largest differences in the sea ice fraction were found.

In the present work, we investigate the dependence of modeled atmospheric boundary layer temperature (ABL) on the sea ice concentration in polar regions. We restrict our study to the cold season during polar night, when we can expect strong convection above leads. For simplicity, we only consider clear-sky conditions keeping in mind, however, that one important factor influencing the ABL energy budget is without any doubt the cloud cover [e.g., *Curry et al.*, 1995]. The lead effect is, however, largest under clear skies in winter, when the surface temperature difference between open leads and thick, snow-covered sea ice can be up to 40 K. Accordingly, the present investigation neglecting clouds represents an estimation of the maximum possible impact of leads. Note also, that cloud-free days occur quite often during arctic winter (e.g., 27 % of all days during the SHEBA ice camp [*Mirocha et al.*, 2005]). We stress that the average effect of leads on climate can only be investigated by taking into account clouds, which would require a more detailed model than we used.

To estimate the impact of leads, a 1D atmospheric model coupled with a thermodynamic sea ice model is used. Lead-induced convective processes are represented similarly as in regional climate models, i.e., the heat emanated from leads is accounted for in the surface fluxes, but no details of the 3D interaction between convective plumes and their environment is modeled. Large-eddy simulations can provide more detailed information on the convection over leads, but our focus is on lead effects in climate and weather prediction models that cannot resolve convective plumes. We consider idealized scenarios (Section 3) with prescribed sea ice and open water (lead) fractions being typical for various regions of the polar oceans.

This study on the impact of leads differs from previous investigations with stand alone sea ice models as those of *Maykut and Untersteiner* [1971] and *Ebert and Curry* [1993]. In their studies, 10-m wind and air temperature were taken from observations or from reanalyses. This procedure does not allow an independent ABL evolution, since the effect of leads on the forcing variables is not accounted for. This drawback is avoided here by prescribing only the geostrophic wind and sea ice fraction.

2. Model description

The atmospheric model is a 1D version of the model METRAS [*Schlünzen*, 1990]. Here, it is important to note that turbulent fluxes in the Ekman layer are determined as in

Lüpkes and Schlünzen [1996] with their nonlocal parameterization allowing countergradient transport of heat and humidity in case of convective conditions. A local mixing length closure is used at neutral and stable conditions [*Vihma et al.*, 2003]. Surface fluxes of momentum, latent and sensible heat are calculated separately for ice and water areas ($F = AF_i + (1 - A)F_w$, where A is the sea ice concentration, F_i and F_w are the surface fluxes over the ice-covered and open-water fractions). Stability functions of Dyer (1974) are used, but we limit the Obukhov length to 10 m for stable stratification. Roughness lengths for momentum are 1 mm and 0.1 mm over ice and water, respectively. The roughness length for heat is one tenth of it. Longwave atmospheric radiative cooling is taken into account prescribing a constant height dependent cooling rate according to *Vihma et al.* [2003]. The model is run with 34 layers, eight layers of which being below 200 m.

The sea ice model consists of 1D diffusion equations solved for the temperatures in the ice and snow layers. The equations are formulated following *Maykut and Untersteiner* [1971], *Ebert and Curry* [1993], and *Makshtas* [1998]. Empirical parameterizations are applied for longwave radiation fluxes with a constant value for the clear-sky emissivity for incoming longwave radiation. The model is run with 1 cm grid size. A sea ice thickness of 2 m is prescribed. Sea ice is covered by a 30 cm snow layer typical for Arctic winter. Since we consider a winter situation and run the model only for a few days, melting effects are neglected. We assume that refrozen leads are replaced by new ones and that A remains constant. The water temperature in leads is also kept constant (271.35 K).

We initialize the model with a temperature profile typically observed over the central Arctic during the cold season, either when clouds prevent longwave radiative cooling of the ABL or as a result of previous warm air advection from regions with less sea ice cover. The temperature profile is characterized by a shallow near-neutral boundary layer capped by a strong inversion at 100 m height. During a complete retreat of clouds we can expect rapid cooling of the sea ice surface and the atmospheric response will strongly depend on the amount of heat released from leads. Model results are generated for different geostrophic wind speeds prescribed to constant values during each run. The results are considered then as a function of the modeled 10-m wind speed at different output times. Results were similar for a prescribed fetch and choosing simulation times according to the ABL wind speed.

3. Results

The air and snow surface temperature after two days simulation time are shown in Figure 1 (bottom) for $A = 95$ % and $A = 100$ %. Temperatures are significantly lower than the initial 250 K, which is due to the radiative cooling. The modeled temperatures strongly depend on A. A decrease of A from 100 % to 95 % causes an increase of up to 18 K ($\approx$ 13 K on average) in the 10-m potential temperature.

Two wind regimes exist with a separating wind speed v_s depending only slightly on A ($v_s = 4.5$ m s^{-1} for $A = 95$ % and $v_s = 4$ m s^{-1} for $A = 100$ %). In the strong-wind regime ($v > v_s$) air and surface temperatures increase with increasing wind speed. This effect turns out to be independent on A, however, it is slightly more pronounced for complete ice cover. In the weak-wind regime ($v < v_s$) the temperature dependence on wind speed differs from that in the strong-wind regime and the behavior of curves depends on A. For A = 100 %, there is a decrease of air and surface temperature with increasing wind speed.

However, for $A = 95$ % the surface temperatures behave as during strong wind, and the two regimes differ mainly by the stability. In the weak-wind regime the difference between the surface and 10-m air temperatures is after 2 days about 2-3 times larger than in the strong-wind regime. The stability in the weak-wind regime increases with decreasing A, until a maximum is reached at about $A = 50$ %, where the temperature difference reaches a value of 8 K (not shown). In the case of complete ice cover such large temperature differences do not occur. Hence, it is obvious that the heat emanating from open water is responsible for this stabilizing effect near the surface.

The role of leads becomes more clear by considering the energy fluxes compiled in Figure 2 for $A = 95$ %. In both wind regimes there is a significant upward sensible heat flux (Figure 2, top) originating from the leads. It is almost linearly increasing with increasing wind speed and compensated by the downward sensible heat flux over the ice areas. Obviously, most of the heat amount originating from leads is returned to the snow surface. Since the downward flux is larger at higher wind speeds, the snow surface temperature is also larger and the ABL temperature maintaining the equilibrium of upward fluxes over water and downward fluxes over ice is increasing as well (Figure 1). The energy budget at the snow surface can only be balanced by the aid of the conductive heat flux. This is important, especially in the weak-wind regime (Figure 2, bottom), where the snow surface is coldest and the temperature gradient through the ice and snow is therefore largest. At $v < v_s$ the downward sensible heat fluxes over ice are relatively small compared with the values for $v > v_s$ and too small to prevent the snow surface from efficient cooling.

Therefore, ABL temperature and surface temperature appear to be decoupled to some extent at weak wind (Figure 1).

In case of complete ice cover the effect of decoupling disappears, at least in the results after two days simulation time, since the near-surface stabilizing effect caused by the heat from leads is missing.

The decrease of air temperature with increasing wind in the weak-wind regime ($A = 1.0$) can be explained with more efficient mixing at higher wind speeds, which leads to an increased loss of heat from the ABL to the surface. With increasing wind, also the snow temperature decreases as downward longwave radiation from the colder air is reduced. This holds only up to the threshold wind speed v_s. At larger wind speeds the increase of temperatures is caused by a growth of ABL thickness z_i (not shown). Its effect can be explained by considering the temperature equation integrated over z_i. Neglecting entrainment and radiation, we obtain

$$\frac{d\theta_m}{dt} = \frac{\overline{w'\theta'}|_s}{z_i} \ ,$$

where θ_m represents the vertically averaged potential temperature in the ABL and $\overline{w'\theta'}|_s$ is the surface heat flux. Hence, a strong increase of z_i decreases the ABL cooling caused by downward flux of sensible heat. Further sensitivity studies demonstrated that this effect is much stronger than that of entrainment.

Clear-sky conditions occur more often for time periods shorter than two days. Thus, results are shown also after twelve hours of simulation (Figure 1, top). Here, the differences between model runs with $A = 100$ % and $A = 95$ % are smaller, but still reach up to 7 K. Furthermore, the decoupling effect between snow and atmosphere at low wind speeds is more pronounced and occurs also for $A = 100$ %. The reason is the initial rapid cooling of the surface and the too slow adjustment of ABL temperatures.

It is noteworthy that the minimum temperature of the snow surface is about 228 K after two days simulation time, a value, which is not far from the minimum temperature (229 K according to *Persson et al.* [2002]) observed during SHEBA. Figure 3 shows 10-m temperatures observed during SHEBA between December 1997 and February 1998 and modeled ones after two days for $A = 99$ %. Detailed observations do not exist for a large region (corresponding to two days of air-mass advection) around the SHEBA site, but 99 % is a typical value for A in the central Arctic during winter. Since we consider clear-sky conditions, our study provides an estimation for extreme cases with the lowest temperatures. Hence, we have to compare the modeled curve with the lowest values for each wind speed during SHEBA. According to Figure 3 these lowest temperatures are well reproduced by the model. Furthermore, also during SHEBA two wind regimes exist with the separating wind speed at 4 m s^{-1}. Hence, the simple model fairly well represents the typical Arctic winter time situation during clear-sky conditions.

Figure 4 shows the modeled 10-m ABL temperatures as a function of prescribed A. Obviously, a small change of A has a strong impact on the ABL temperature. The curve steepens with increasing simulation time. A change of 1 % in A results in roughly 1 K and 3.5 K change of the ABL temperature after 12 and 48 hours simulation time, respectively.

The sensitivity of results on atmospheric longwave radiative cooling was also tested. However, the structure of curves in Figures 1 and 4 remained unchanged. The new temperature curves were simply shifted parallel to the former ones.

4. Discussion and conclusions

Obviously, there is a strong sensitivity of the results to the lead (or open water) fraction. The strong dependence of ABL temperature on the sea ice fraction demonstrates the need for very accurate observations of sea ice concentration A in the central polar regions. This generates a challenge for the development of remote sensing methods, since the present ones that can provide daily data with extensive spatial coverage are not accurate enough for A exceeding 90 % [e.g., *Andersen et al.*, 2007]. Furthermore, erroneous sea ice concentrations obtained from climate models could have a strong impact on their results.

Our results suggest that for $A = 95$ % the upward sensible heat flux from leads practically balances the downward flux over ice. Observations support this finding: *Overland et al.* [2000] draw analogous conclusions on the basis of analyses of SHEBA meteorological measurements and remote sensing data on the snow surface temperature in winter clear-sky conditions. We stress that the near-zero area-averaged heat flux is received via the significant lead effect on the ABL temperature.

Another important result consists of the existence of two wind regimes, which were modeled and also found in the SHEBA data. Our further sensitivity studies (not shown) revealed that the existence of the weak-wind regime depends on the surface layer stability function for stable stratification. E.g., stability functions allowing larger sensible heat fluxes directed to sea ice allow also a faster adjustment between air and snow surface temperature with a smaller value of v_s. Nevertheless, with the presently applied functions this adjustment was modeled earlier in good agreement to observations [*Vihma et al.*, 2003]. Furthermore, decoupling of the atmosphere from the underlying surface at stable stratification during low winds is a phenomenon often observed in polar regions e.g., over sea ice in the SHEBA experiment [*Grachev et al.*, 2005]. Our model results also suggest that the effect of leads in further stabilizing the lowest tens of meters of air over sea ice is important in maintaining the decoupling over periods of up to two days. This has not been addressed earlier.

The present estimations are valid for the polar night under clear-sky conditions. In overcast conditions over the Arctic sea ice the snow surface temperature is about 15 K warmer [*Vihma and Pirazzini*, 2005]. The surface temperature difference between leads and sea ice is accordingly strongly reduced, which dampens the lead effect on the ABL.

There are certainly additional factors influencing the ABL temperature, which were not considered so far. Besides clouds the most important one is horizontal advection. It may overlay the considered cooling/heating rates and should be included into future investigations. Finally, the results depend also on the initial conditions, on parameters like sea ice thickness, snow thickness, surface roughness, and the prescribed initial boundary layer depth. However, it turned out from additional model runs that the variation of all these parameters hardly changes our conclusions.

Acknowledgments. This study was supported by the EU project DAMOCLES (grant no. 18509), which is part of the Sixth Framework Programme, by DFG (grant no. LU 818/1-1) and by the Academy of Finland (grant 210794). Observations shown in Figure 3 were made by the SHEBA Atmospheric Surface Flux Group, Ed Andreas, Chris Fairall, Peter Guest, and Ola Persson.

References

Arctic Climate Impact Assessment (ACIA) (2005), Chapter 6: Cryosphere and Hydology, John E. Walsh et al., Cambridge University Press, www.acia.uaf.edu, 184–236.

Curry, J., Schramm, J.L., Serreze, M.C., and E.E. Ebert (1995), Water vapor feedback over the Arctic ocean, *J. Geophys. Res.*, 100(D7), 14,223–14,229.

Dyer, A.J. (1974), A review of flux-profile relationship, *Boundary-Layer Meteorol.*, 7, 363–372.

Ebert, E.E., and J.A, Curry (1993), An intermediate one-dimensional thermodynamic sea ice model for investigating ice-atmosphere interactions, *J. Geophys. Res.*, 98(C6), 10085–10109.

Grachev, A.A., Fairall, C.W., Persson, P.O.G., Andreas, E.L., and P.S. Guest (2005), Stable boundary-layer regimes: The SHEBA data, *Boundary-Layer Meteorol.*, 116, 201-235.

Lüpkes, C. and K.H. Schlünzen (1996), Modelling the Arctic convective boundary-layer with different turbulence parameterizations, *Boundary-Layer Meteorol.*, 79, 107–130.

Makshtas, A.P. (1998), Thermodynamics of sea ice, in *Physics of ice-covered seas*, edited by M. Leppäranta, pp. 289-303, University Printing House, Helsinki.

Maykut, G.A., and N. Untersteiner (1971), Some results from a time dependent thermodynamic model of sea ice, *J. Geophys. Res.*, 76(6), 1550–1575.

Mirocha, J.D., Kosovic, B., and J. Curry (2005), vertical heat transfer in the lower atmosphere over the Arctic ocean during clear-sky periods, Boundary-Layer Meteorol., 117, 37–71.

Overland, J. E., McNutt, S. L., Groves, J., Salo, S., Andreas, E. L., and P. O. G. Persson (2000), Regional sensible and radiative heat flux estimates for the winter Arctic during the Surface Heat Budget of the Arctic Ocean (SHEBA) experiment, J. Geophys. Res., 105 (C6), 14093–14102.

Schlünzen, K. H. (1990), Numerical studies on the inland penetration of sea breeze fronts at a coastline with tidally flooded mudflats, *Beitr. Phys. Atmosph.*, 63, 243–256.

Sorteberg, A., Kattsov, V., Walsh, J.E., and T. Pavlova (2007), The Arctic surface energy budget as simulated with the IPCC AR4 AOGCMs, *Clim. Dyn.*, 29, 131–156.

Vihma, T., Hartmann, J. and C. Lüpkes (2003), A case study of an on-ice air flow over the Arctic marginal sea ice zone, *Boundary-layer Meteorol.*, 107,189–217.

Vihma, T., and R. Pirazzini (2005), On the factors controlling the snow surface and 2-m air temperatures over the Arctic sea ice in winter, *Boundary-layer Meteorol.*, 117,73–90.

5. Figures

Figure 1: Modeled snow surface temperature (blue) and 10-m air potential temperature (red).

Figure 2: Top: area averaged surface fluxes in the atmosphere model for $A = 95$ % after two days simulation time. Bottom: fluxes in the snow/ice model related only to the ice covered area (downward fluxes are negative).

Figure 3: 10-m air temperature observed during SHEBA between December 1997 and February 1998 (black symbols) and model results for $A = 99$ % after two days (blue).

Figure 4: Model results after 12 hours (open symbols) and after two days (closed symbols) simulation time.

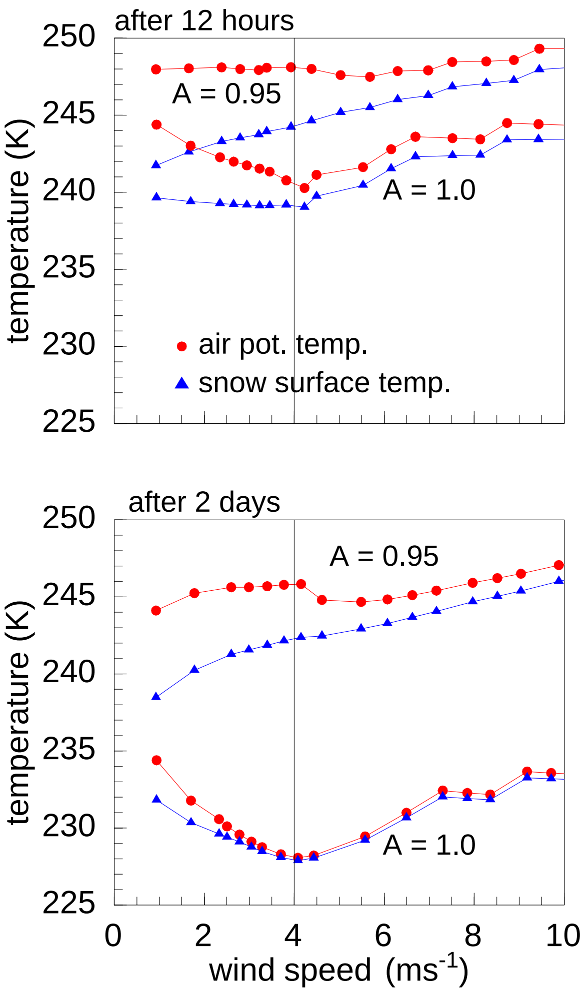
after 12 hours
250
245
240
235
230
225
temperature (K)
A = 0.95
A = 1.0
air pot. temp.
snow surface temp.
after 2 days
A = 0.95
A = 1.0
0
2
4
6
8
10
wind speed (ms-1)

244 Fig. 1

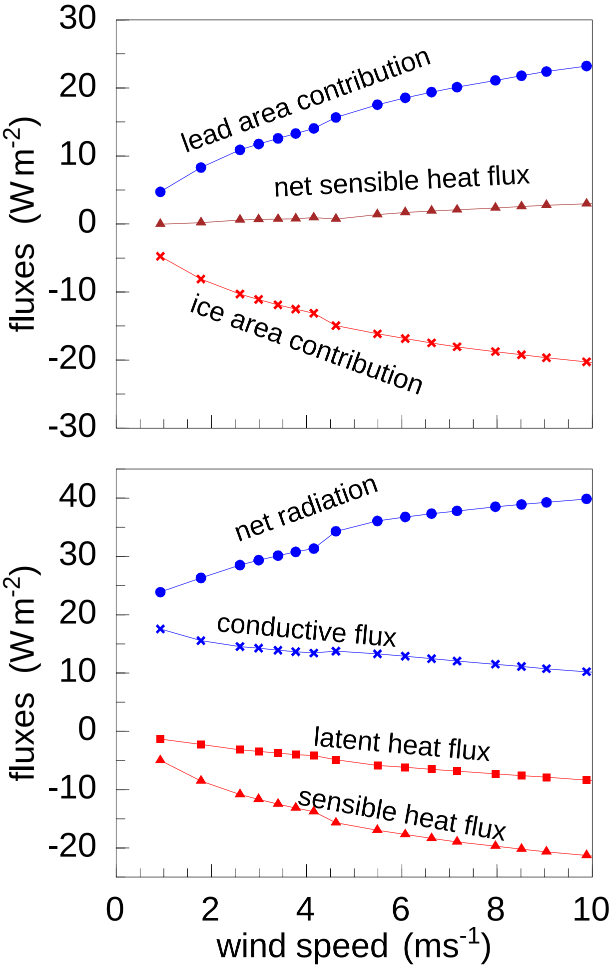
30
20
10
0
-10
-20
-30
fluxes (W m-2)
lead area contribution
net sensible heat flux
ice area contribution
40
30
20
10
0
-10
-20
fluxes (W m-2)
net radiation
conductive flux
latent heat flux
sensible heat flux
0
2
4
6
8
10
wind speed (ms-1)

245 Fig. 2

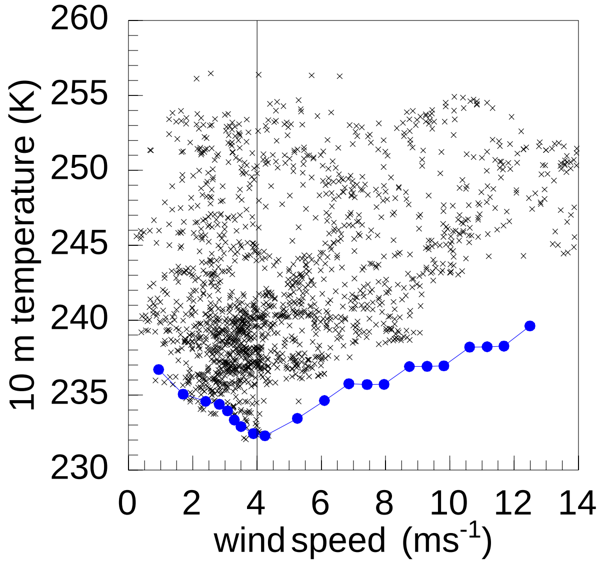
260
255
250
245
240
235
230
10 m temperature (K)
0
2
4
6
8
10
12
14
wind speed (ms-1)

246 Fig. 3

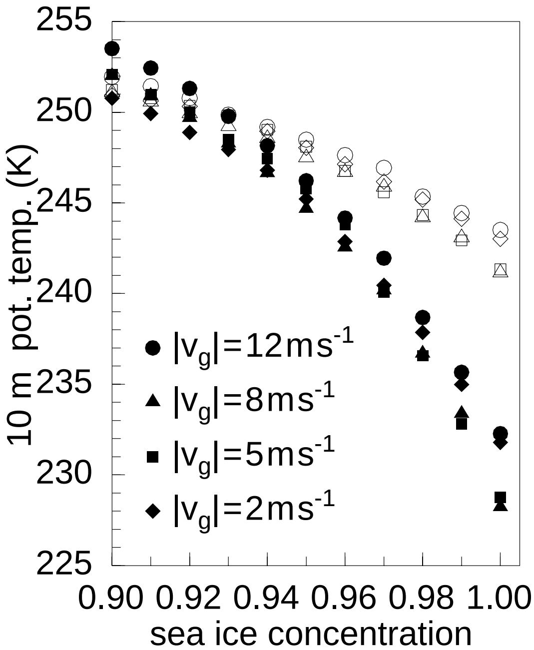
255
250
245
240
235
230
225
10 m pot. temp. (K)
$|v_g|=12ms^{-1}$
$|v_g|=8ms^{-1}$
$|v_g|=5ms^{-1}$
$|v_g|=2ms^{-1}$
0.90 0.92 0.94 0.96 0.98 1.00
sea ice concentration

247 Fig. 4